Three-Dimensional Guidance Law Mimicking Realistic Ballistic Trajectories

Article *in* Journal of Guidance, Control, and Dynamics · May 2022

DOI: 10.2514/1.G006741

CITATION
1

READS
767

3 authors, including:

Robert Fonod
École Polytechnique Fédérale de Lausanne
35 PUBLICATIONS **424** CITATIONS
SEE PROFILE

Spilios Theodoulis
Deutsch-Französisches Forschungsinstitut Saint-Louis
46 PUBLICATIONS **475** CITATIONS
SEE PROFILE

Three-Dimensional Guidance Law Mimicking Realistic Ballistic Trajectories

Robert Fonod *, Michael Proff †, and Spilios Theodoulis‡
French-German Research Institute of Saint-Louis, Saint-Louis, 68300, France

I. Introduction

Development of guidance and control for precision-guided projectiles is an active field of research that has emerged from increasing operational requirements of guided ammunition in range, accuracy, and cost [1, 2]. Gun-launched projectiles follow a ballistic trajectory to reach their target. Impact accuracy can be significantly affected by uncertainties in modeling aerodynamic characteristics and unknown atmospheric perturbations. Due to the severely limited maneuverability of aerodynamically controlled projectiles, designing guidance laws that mimic realistic ballistic trajectories is of great interest. Modern projectile guidance laws generally follow one of the three design paradigms: trajectory following, trajectory shaping, or predictive guidance [3].

Trajectory tracking [3–5] aims at minimizing the in-flight error between the expected ballistic trajectory and the actual position of the projectile. The tracked trajectory is uploaded into the projectile prior to or at launch. This type of guidance logic is easy to implement, requires low computing power, and allows retaining the general ballistic tables [3]. On the other hand, it tends to be less robust and requires a higher level of maneuverability than predictive guidance [6].

Traditional trajectory shaping algorithms may force the projectile to follow non-ballistic trajectories and typically require high control effort [3], often resulting in energy-inefficient actuation force distribution over the trajectory, which can produce undesired actuator saturations [3]. The Proportional Navigation (PN) guidance law [7] is perhaps one of the most popular trajectory shaping guidance laws designed to intercept stationary or low-speed targets. Despite its implementation simplicity, is not well suited for gun-launched projectiles, unless it is employed during the terminal phase. There have been several efforts to adapt the PN scheme to account for the curvature of the ballistic trajectory [8–11]. Guo et al. [8] suggested a heuristic multi-stage guidance approach for dual-spin projectiles. The first stage is employed at the ascending phase and consists of a parameter-varying lateral deviation correction scheme only, while the second stage is engaged at the descending phase and employs a conventional constant-gain PN guidance scheme for simultaneous lateral and longitudinal corrections. Zhang et al. [9] proposed an adaptive variant of the 2D PN guidance law suitable for curved trajectories in the vertical plane. The variable guidance gain is computed off-line based on the nominal ballistic trajectory and uploaded into the projectile, where it is later retrieved from a lookup table using the projectile's actual longitudinal position. Finally, Sharma and Ratnoo [10] derived an adaptive 2D PN-like guidance

*Research Scientist, Department of Guidance, Navigation, and Control, robert.fonod@ieee.org (Corresponding Author).
†Research Engineer, Department of Guidance, Navigation, and Control, Michael.Proff@isl.eu, AIAA Member.
‡Senior Research Scientist, Department of Guidance, Navigation, and Control, Spilios.Theodoulis@isl.eu, AIAA Senior Member.

scheme to mimic short-range ballistic trajectories. In contrast to [9], the coefficients determining the time-varying guidance gain were derived analytically and evaluated in-flight using bearings-only information. This method has been later extended by the same authors to take into account look-angle constraints [11].

Predictive guidance uses a ballistic model to predict the impact point of the projectile and compute corrections accordingly. Impact Point Prediction (IPP) based guidance laws were used to improve guidance performance for gun-launched projectiles [6, 12–14]. Alongside evaluating aerodynamic data, the EoM need to be solved in real-time for each guidance update instant, leading to a high on-board computation burden. Several attempts have been made to reduce the computational burden of IPP-based methods. Yang [12] proposed an IPP method based on solving algebraic equations based on the estimated location, velocity, and acceleration of a spinning projectile. IPP based on perturbation theory was proposed in [13] for projectiles with 2D trajectory correction fuse. Gagnon and Vachon [6] proposed an improved IPP method for spin-stabilized projectiles. The method leverages the Modified Point Mass (MPM) model of [15] with an additional term for spin rate. The additional term aims at taking into account the drift in the crossrange direction due to the yaw of repose. Proff and Theodoulis [14] further improved the MPM model by assuming variable spin rate, variable aerodynamic parameters, and variable angle of repose. The IPP based on the improved MPM model of [14] was implemented using the so-called Zero-Effort-Miss (ZEM) guidance formulation and is referred to in this paper as the state-of-the-art guidance method.

Despite the implementation simplicity of the existing trajectory shaping guidance laws, their main disadvantage is the inability to adequately account for the drift in the crossrange direction. On the other hand, predictive guidance methods are able to account for this issue, but they require high on-board computing capabilities. In this paper, we aim at combining the benefits of these two guidance paradigms. We propose a new practical three-dimensional (3D) guidance law suitable for a large class of gun-launched spin-stabilized or fin-stabilized projectiles. The proposed law aims at mimicking a realistic ballistic trajectory by adapting the navigation gain of the conventional PN guidance law to produce acceleration load factor commands similar to the ones experienced by an unguided projectile flying on a nominal trajectory. Consequently, the resulting guidance strategy achieves the accuracy of state-of-the-art predictive methods while maintaining a relatively simple implementation complexity, low on-board computational burden, and reduced maneuverability requirements, ideal for low maneuverability canard-guided projectiles.

II. Background

A. Overview of Applicable Concepts

The guidance schemes discussed in this paper are applicable to a wide family of gun-launched fin-stabilized and spin-stabilized guided projectiles. The presented concept potentially allows to consider canard or tail control approaches. Fin-stabilized projectiles rely on aerodynamic surfaces for stability and control, and resemble more to missile systems,

albeit demonstrating less maneuverability. On the other hand, spin-stabilized guided projectiles are typically equipped with a roll-decoupled course correction fuse (CCF), designed to provide range and/or lateral corrections, while at the same time, they rely on the high spin rate of the aft part for gyroscopic and potential dynamic stability.

An example of a dual-spin canard-guided projectile concept is illustrated in Fig. 1, along with a dedicated reference frame and some flight mechanics state variables, both of which will be described further down. The aft part typically houses the payload and spins freely, while the front part accommodates a set of canards used for aerodynamic trajectory correction. The fuze also contains all the necessary GNC software and hardware, such as g-hardened inertial measurement units (IMUs), Global Navigation Satellite System (GNSS) receivers, and on-board computing units. The main shortcoming of CCF projectiles is their very limited maneuverability. Since the maximum acceleration that a typical CCF projectile can generate is way less than the amount needed to counteract gravity.

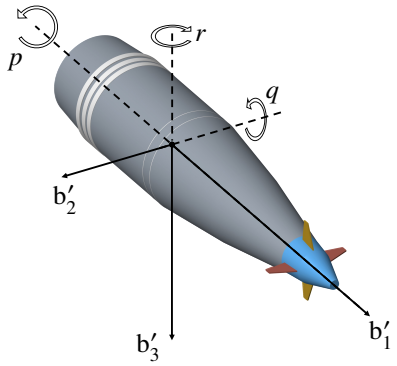

Fig. 1 ISL's 155 mm course correction fuze concept. Adapted from [16]. ©2020 by French-German Research Institute of Saint-Louis.

B. Frames and Coordinate Systems

Several right-handed orthonormal frames and their associated Cartesian coordinate systems will be used throughout this paper. Neglecting the Coriolis and centrifugal forces, the Earth is chosen as an inertial reference frame E by unwrapping and centering the Earth's surface into a plane tangential to the launch point E (flat-Earth approach). The right-handed orthonormal triad of base vectors $(\boldsymbol{e}_1, \boldsymbol{e}_2, \boldsymbol{e}_3)$ and the base point E of this frame is illustrated in Fig. 2. The $\boldsymbol{e}_1$ axis points northwards, $\boldsymbol{e}_3$ axis is parallel and in the direction of the gravity vector, and $\boldsymbol{e}_2$ completes the triad by pointing eastwards. The body-fixed (rolling) frame B is centered at the projectile's Center of Mass (CoM) B and defined by the triad $(\boldsymbol{b}_1, \boldsymbol{b}_2, \boldsymbol{b}_3)$. The $\boldsymbol{b}_1$ axis points towards the projectile nose, $\boldsymbol{b}_2$ is normal to $\boldsymbol{b}_1$ and points rightwards, and $\boldsymbol{b}_3$ points downwards and is normal to $\boldsymbol{b}_1 - \boldsymbol{b}_2$. The body non-rolling (BNR) frame B′ is an intermediate frame also centered at the projectile CoM B and defined by the triad $(\boldsymbol{b}'_1, \boldsymbol{b}'_2, \boldsymbol{b}'_3)$. Its second base vector $\boldsymbol{b}'_2$ lies always on the horizontal $\boldsymbol{e}_1 - \boldsymbol{e}_2$ plane and is normal to $\boldsymbol{b}_1$, $\boldsymbol{b}'_1 \equiv \boldsymbol{b}_1$, and $\boldsymbol{b}'_3$ completes the triad. Unlike B, the BNR frame B′ will only experience pitching and yawing angular motions, but not the rolling motion. The target-fixed frame T is centered at

the target's CoM T. The definition of the basis vectors for T can be arbitrary and depends on its type. The flight-path frame V is defined by the triad $(\boldsymbol{v}_1, \boldsymbol{v}_2, \boldsymbol{v}_3)$. The $\boldsymbol{v}_1$ vector is parallel and in the direction of the velocity vector of the projectile wrt the flat-Earth $\boldsymbol{v}_{\mathrm{B}}^{\mathrm{E}}$, the $\boldsymbol{v}_2$ vector remains in the horizontal plane subtended by $\boldsymbol{e}_1$ and $\boldsymbol{e}_2$, $\boldsymbol{v}_3$ completes the triad. Finally, the line-of-sight (LoS) frame O is defined by the triad $(\boldsymbol{o}_1, \boldsymbol{o}_2, \boldsymbol{o}_3)$. The $\boldsymbol{o}_1$-direction is parallel and in the direction of the LoS vector $\boldsymbol{s}_{\mathrm{TB}}$, a vector connecting B with T; the $\boldsymbol{o}_2$-direction is normal to $\boldsymbol{o}_1$ and lies in the $\boldsymbol{e}_1 - \boldsymbol{e}_2$ plane; and $\boldsymbol{o}_3$ completes the triad. Both, O and V, have their base point at the projectile CoM B.

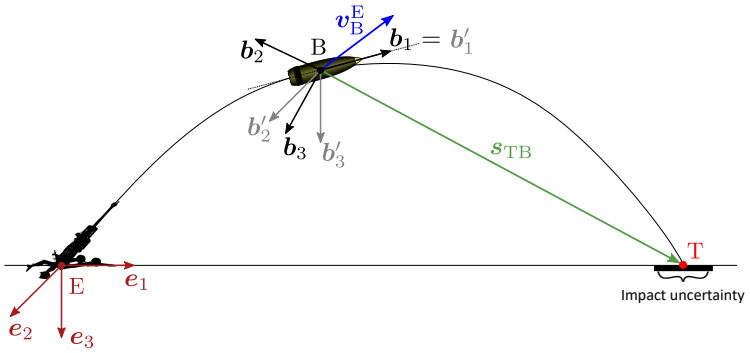

Fig. 2 Illustration of the employed reference frames.

The local-level Coordinate System (CS), $]^{\mathrm{L}}$, also known as the North-East-Down or NED, is the preferred CS for E. Similarly, the preferred CS for B, B′, T, V, and O, respectively, is $]^{\mathrm{B}}$, $]^{\mathrm{B}'}$,$]^{\mathrm{T}}$, $]^{\mathrm{V}}$, and $]^{\mathrm{O}}$. The axes of all these coordinate systems line up with the base vectors of the frames they are associated to. Figure 3 depicts the orientation between selected coordinate systems, including the associated transformation angles as well as intermediate systems $]^{\mathrm{X}}$ and $]^{\mathrm{Y}}$, where applicable. Specifically, Fig. 3a follows the aircraft Euler angle convention. Two rotations are needed in order to pass from $]^{\mathrm{L}}$ to $]^{\mathrm{B}'}$. The first by the yaw angle ψ, and the second by the pitch angle θ. The third rotation by the roll angle ϕ takes us to $]^{\mathrm{B}}$, the CS needed for control purposes (e.g., to compute the canards deflection angles). The meaning and definition of angles shown in Fig. 3b and Fig. 3c will become evident in Section III.

C. Nonlinear Dynamics and Kinematics

A generic 6 degrees of freedom (DoF) nonlinear model of the projectile's dynamics and kinematics is introduced here. This model is suitable for simulating the 3D trajectory of a spin-stabilized or a fin-stabilized projectile and will be used later for guidance design. The projectile EoM are expressed using the BNR frame B′ rather than the conventional body-fixed frame B that would roll along with the body. This is especially advantageous for roll-symmetric spin-stabilized projectiles, where the high spin rate (typically between 170 and 300 Hz) would require a very small integration step to capture the true underlying roll dynamics. This would ultimately result in long simulation times and may lead to large accumulated numerical errors [17].

The EoM of the translational and attitude airframe dynamics, coordinated to the BNR CS $]^{\mathrm{B}'}$, are given by*

*Capital subscripts denote points while capital superscripts signify frames. Two subscripts or superscripts are read from left to right, inserting the

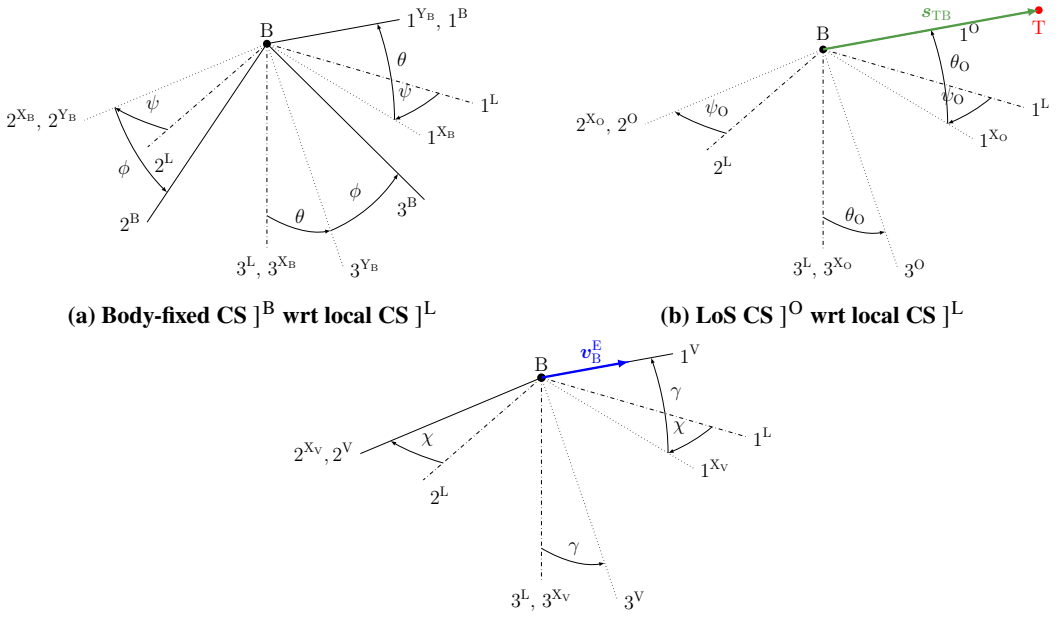

(a) Body-fixed CS $]^B$ wrt local CS $]^L$

(b) LoS CS $]^O$ wrt local CS $]^L$

(c) Flight-path CS $]^V$ wrt local CS $]^L$

Fig. 3 Orientation and associated transformation angles between selected coordinate systems.

$$m\left[\dot{\boldsymbol{v}}_{\mathrm{B}}^{\mathrm{E}}\right]^{\mathrm{B}'} + m\left[\boldsymbol{\Omega}^{\mathrm{B}'\mathrm{E}}\right]^{\mathrm{B}'}\left[\boldsymbol{v}_{\mathrm{B}}^{\mathrm{E}}\right]^{\mathrm{B}'} = \left[\boldsymbol{f}_{\mathrm{a,g}}\right]^{\mathrm{B}'}, \tag{1}$$

$$\left[\boldsymbol{I}_{\mathrm{B}}^{\mathrm{B}}\right]^{\mathrm{B}'}\left[\dot{\boldsymbol{\omega}}^{\mathrm{BE}}\right]^{\mathrm{B}'} + \left[\boldsymbol{\Omega}^{\mathrm{B}'\mathrm{E}}\right]^{\mathrm{B}'}\left[\boldsymbol{I}_{\mathrm{B}}^{\mathrm{B}}\right]^{\mathrm{B}'}\left[\boldsymbol{\omega}^{\mathrm{BE}}\right]^{\mathrm{B}'} = \left[\boldsymbol{m}_{\mathrm{a}}\right]^{\mathrm{B}'}. \tag{2}$$

The components of linear velocity ($\boldsymbol{v}_{\mathrm{B}}^{\mathrm{E}}$), angular velocity ($\boldsymbol{\omega}^{\mathrm{BE}}$), aerodynamic and gravity forces ($\boldsymbol{f}_{\mathrm{a,g}}$), and aerodynamic moments referred to the CoM ($\boldsymbol{m}_{\mathrm{a}}$), are defined, respectively, as[†]

$$\left[\boldsymbol{v}_{\mathrm{B}}^{\mathrm{E}}\right]^{\mathrm{B}'} \triangleq \begin{bmatrix} u \\ v \\ w \end{bmatrix}, \quad \left[\boldsymbol{\omega}^{\mathrm{BE}}\right]^{\mathrm{B}'} \triangleq \begin{bmatrix} p \\ q \\ r \end{bmatrix}, \quad \left[\boldsymbol{f}_{\mathrm{a,g}}\right]^{\mathrm{B}'} \triangleq \begin{bmatrix} X \\ Y \\ Z \end{bmatrix}, \quad \left[\boldsymbol{m}_{\mathrm{a}}\right]^{\mathrm{B}'} \triangleq \begin{bmatrix} L \\ M \\ N \end{bmatrix}.$$

The externally-applied airframe forces (X, Y, Z) contain a sum of gravitational and aerodynamic components. The aerodynamic components are due to drag-lift, damping, Magnus (for spinning projectiles only), and control forces. The externally-applied airframe moments (L, M, N) are a result of these aerodynamic forces and internal mechanical friction, if applicable. In (1), m signifies the projectile mass. In (2), $\left[\boldsymbol{I}_{\mathrm{B}}^{\mathrm{B}}\right]^{\mathrm{B}'}$ stands for the moment of inertia (MoI) of the projectile body B referred to the its CoM B and expressed in the CS $]^{\mathrm{B}'}$. Finally, the skew-symmetric matrix form of

word "relative to" [18]. For sake of clarity, the notation of time-dependency (t) of some variables is omitted whenever the context is clear.

[†]By standard frame notation conventions, we should write u', v', w', p', etc., but for sake of notational simplicity, we drop the '′' notation.

the angular velocity of B′ wrt E expressed in $]^{\mathrm{B}'}$ is

$$\left[\boldsymbol{\Omega}^{\mathrm{B}'\mathrm{E}}\right]^{\mathrm{B}'} = \begin{bmatrix} 0 & -r & q \\ r & 0 & r\tan\theta \\ -q & -r\tan\theta & 0 \end{bmatrix}.$$

The translational and attitude kinematics, coordinated into $]^{\mathrm{L}}$ and expressed using Euler angles convention, respectively, are given by

$$[\dot{\boldsymbol{s}}_{\mathrm{BE}}]^{\mathrm{L}} = \left[\bar{\boldsymbol{T}}\right]^{\mathrm{B}'\mathrm{L}} \left[\boldsymbol{v}_{\mathrm{B}}^{\mathrm{E}}\right]^{\mathrm{B}'}, \tag{3}$$

$$\dot{\boldsymbol{e}}^{\mathrm{BE}} = \boldsymbol{J}^{e\omega} \left[\boldsymbol{\omega}^{\mathrm{BE}}\right]^{\mathrm{B}'}. \tag{4}$$

The components of the linear position $(\boldsymbol{s}_{\mathrm{BE}})$, angular position $(\boldsymbol{e}^{\mathrm{BE}})$, and the matrix $\boldsymbol{J}^{e\omega}$ are

$$[\boldsymbol{s}_{\mathrm{BE}}]^{\mathrm{L}} \triangleq \begin{bmatrix} x \\ y \\ z \end{bmatrix}, \quad \boldsymbol{e}^{\mathrm{BE}} \triangleq \begin{bmatrix} \phi \\ \theta \\ \psi \end{bmatrix}, \quad \boldsymbol{J}^{e\omega} = \begin{bmatrix} 1 & 0 & \tan\theta \\ 0 & 1 & 0 \\ 0 & 0 & \sec\theta \end{bmatrix}.$$

Finally, the orthogonal time-dependent coordinate transformation matrix $[\boldsymbol{T}]^{\mathrm{B}'\mathrm{L}}$ in (3) is given as a function of the projectile pitch θ and yaw ψ Euler angles, i.e.,

$$\left[\bar{\boldsymbol{T}}\right]^{\mathrm{B}'\mathrm{L}} = \begin{bmatrix} \cos\theta\cos\psi & -\sin\psi & \sin\theta\cos\psi \\ \cos\theta\sin\psi & \cos\psi & \sin\theta\sin\psi \\ -\sin\theta & 0 & \cos\theta \end{bmatrix}, \tag{5}$$

where the overbar indicates matrix transpose.

III. Guidance Law Design

A. Problem Formulation

The role of a guidance algorithm is to generate suitable reference pitch/yaw-channel load factor orders. Canard or fin deflections are usually used as control surfaces. The normal $n_{\mathrm{z,cmd}}$ and lateral $n_{\mathrm{y,cmd}}$ load factor commands are used

as a tracking outputs for the autopilot and are defined in this paper as follows:

$$\begin{bmatrix} n_{\mathrm{z,cmd}} \\ n_{\mathrm{y,cmd}} \end{bmatrix} = \frac{1}{g(h)} \begin{bmatrix} 0 & 0 & 1 \\ 0 & 1 & 0 \end{bmatrix} \left[\boldsymbol{a}_{\mathrm{B}}^{\mathrm{E}}\right]_{\mathrm{cmd}}^{\mathrm{B}'}. \tag{6}$$

Here, the two selected components of the 3D acceleration command $\left[\boldsymbol{a}_{\mathrm{B}}^{\mathrm{E}}\right]_{\mathrm{cmd}}^{\mathrm{B}'}$, which will be designed later, are converted to units in g's and sent to the autopilot in order to steer the projectile with accuracy to the target [18]. The third component parallel to the body is normally unused, unless a so-called *braking function* is available to the projectile, see Gagnon and Lauzon [3] and references therein. In (6), $g(h)$ stands for the altitude ($h \triangleq -z$) dependent acceleration due to the gravity. In this paper, a simplified first-order linear regression model is adopted,

$$g(h) = G\frac{M}{r^2} \approx g_0 + g_1 h, \tag{7}$$

where M is the mass of Earth, r is the distance from Earth center, and G is the universal gravitational constant. The numerical values for g_0 and g_1 are considered as follows: $g_0 \doteq 9.8084$ [m/s^2] and $g_1 \doteq -3.0710 \times 10^{-6}$ [1/s^2].

In order to avoid actuator saturation and/or autopilot instability, a *flight envelope protection* function $f_p(\cdot)$ is often applied to the load factor commands (6), i.e., for $\mathrm{i} \in \{\mathrm{y}, \mathrm{z}\}$, we have

$$f_p(n_{\mathrm{i,cmd}}) = \begin{cases} n_{\mathrm{i,cmd}} & \text{if } |n_{\mathrm{i,cmd}}| \le \bar{n}_{\mathrm{i}}(h, V), \\ \mathrm{sign}(n_{\mathrm{i,cmd}})\bar{n}_{\mathrm{i}}(h, V) & \text{else,} \end{cases} \tag{8}$$

where $\bar{n}_{\mathrm{i}}(h, V)$ is, in general, the altitude h and speed $V \triangleq \sqrt{u^2 + v^2 + w^2}$ dependent load factor order limit in g's.

B. Proportional Navigation

Adopted from physical intuition, the PN guidance law is perhaps one of the most common guidance laws in use, particularly for air-to-air engagements. The acceleration command of the gravity-compensated 3D pure PN guidance law, expressed in the CS $]^{\mathrm{B}'}$, is given by [18]

$$\left[\boldsymbol{a}_{\mathrm{B}}^{\mathrm{E}}\right]_{\mathrm{cmd}}^{\mathrm{B}'} = N\left[\boldsymbol{\omega}^{\mathrm{OE}}\right]^{\mathrm{B}'} \times \left[\boldsymbol{v}_{\mathrm{B}}^{\mathrm{E}}\right]^{\mathrm{B}'} - [\boldsymbol{T}]^{\mathrm{B}'\mathrm{L}}[\boldsymbol{g}]^{\mathrm{L}}, \tag{9}$$

where N is the so-called *navigation gain* and $[\boldsymbol{g}]^{\mathrm{L}}$ is the gravitational acceleration vector in the local-level CS $]^{\mathrm{L}}$, defined as

$$[\boldsymbol{g}]^{\mathrm{L}} \triangleq \begin{bmatrix} 0 \\ 0 \\ g(h) \end{bmatrix}, \tag{10}$$

and transformed into the BNR CS using the transformation matrix $[\boldsymbol{T}]^{\mathrm{B'L}}$. The angular rate tensor of O wrt E expressed in $]^{\mathrm{B'}}$ is given by

$$\left[\boldsymbol{\omega}^{\mathrm{OE}}\right]^{\mathrm{B'}} = [\boldsymbol{T}]^{\mathrm{B'L}} \left[\boldsymbol{\omega}^{\mathrm{OE}}\right]^{\mathrm{L}} = [\boldsymbol{T}]^{\mathrm{B'L}} \frac{\left[\boldsymbol{s}_{\mathrm{TB}}\right]^{\mathrm{L}} \times \left[\boldsymbol{v}_{\mathrm{TB}}^{\mathrm{E}}\right]^{\mathrm{L}}}{\left\|[\boldsymbol{s}_{\mathrm{TB}}]^{\mathrm{L}}\right\|^2}, \tag{11}$$

where $\|\cdot\|$ stands for the Euclidean norm of a vector and $\boldsymbol{s}_{\mathrm{TB}}$ is the relative displacement of the target CoM T wrt the projectile CoM B. Coordinating $\boldsymbol{s}_{\mathrm{TB}}$ to CS $]^{\mathrm{L}}$, we have

$$[\boldsymbol{s}_{\mathrm{TB}}]^{\mathrm{L}} \triangleq [\boldsymbol{s}_{\mathrm{TE}}]^{\mathrm{L}} - [\boldsymbol{s}_{\mathrm{BE}}]^{\mathrm{L}}. \tag{12}$$

Here, $\boldsymbol{s}_{\mathrm{TB}}$ is also referred to as the LoS vector, see Fig. 2. The target's inertial position $\boldsymbol{s}_{\mathrm{TE}}$ is considered to be perfectly known and fixed through the engagement. The differential velocity vector,

$$\left[\boldsymbol{v}_{\mathrm{TB}}^{\mathrm{E}}\right]^{\mathrm{L}} \triangleq \left[\boldsymbol{v}_{\mathrm{T}}^{\mathrm{E}}\right]^{\mathrm{L}} - \left[\boldsymbol{v}_{\mathrm{B}}^{\mathrm{E}}\right]^{\mathrm{L}} = -\left[\boldsymbol{v}_{\mathrm{B}}^{\mathrm{E}}\right]^{\mathrm{L}}, \tag{13}$$

is the differential velocity of the target T wrt the projectile B as observed from E. In this paper, only stationary targets are considered, hence $\boldsymbol{v}_{\mathrm{T}}^{\mathrm{E}}$ in (13) is considered zero. This is a deliberate choice of the authors since the class of projectiles studied here does not have either the necessary maneuverability or the on-board sensors (for example seekers) to detect and intercept moving targets.

C. Ballistic Proportional Navigation

In case of a stationary target, the PN guidance law is able to intercept the target with zero miss distance by any $N > 0$, provided perfect navigation information, instantaneous execution of the requested load factor commands, and no maneuverability limitations. Specifically, the last assumption poses a serious challenge for canard-guided projectiles, which often have very limited maneuvering capabilities [19].

In missile guidance applications, the gain N is normally assumed constant and typically takes values between 3 and 5 [20]. The higher the value, the closer the resulting trajectory to the straight-line [21]. Obviously, this is in contradiction to the natural ballistic flight path curvature typical for gun-launched projectiles (cf. Fig. 2 for illustration).

During the terminal phase of a ballistic flight, the resulting trajectory resembles a quasi straight-line, approaching the

validity of the underlying assumptions used in the PN guidance law derivation (e.g., the engagement geometry staying close to the collision course [21]). Therefore, the baseline PN guidance law is typically only engaged during the terminal guidance phase of gun-launched projectiles. For low maneuverability projectiles, lower guidance gains, i.e., $N < 3$, were suggested in order to limit the risk of canards saturation while maintaining acceptable impact accuracy [19].

In this paper, we introduce three alternatives to the conventional constant-gain 3D PN guidance law. Henceforth, we will refer to these alternatives as: 1) Ideal Ballistic Proportional Navigation (IBPN); 2) IBPN with look-angle Constraints (IBPN+C); and 3) Realistic Ballistic Proportional Navigation (RBPN). For each alternative, we aim to preserve the relatively simple structure of the PN guidance law introduced in (9). However, instead of using a constant navigation gain N, the goal is to design a time-varying alternative $N(t)$ that shapes the 3D trajectory of a guided projectile to mimic a ballistic one. Consequently, this scheme should be able to engage a closed-loop guidance strategy much earlier.

1. Ideal Ballistic Proportional Navigation

As the name suggests, IBPN aims at mimicking a ballistic trajectory under ideal ballistic trajectory assumptions, i.e., no lift, drag or side forces. Sharma and Ratnoo [10] derived in closed-form a time-varying navigation gain for a planar 2D engagement, which can be expressed as follows:

$$N(t) = k_1 - k_2\theta_{\mathrm{O}}(t), \qquad t \in [t_0, t_{\mathrm{f}}), \tag{14}$$

where θ_{O} is the LoS elevation angle (cf. Fig. 3b) defined as

$$\theta_{\mathrm{O}} = \arctan\left(\frac{-z_{\mathrm{TB}}}{\sqrt{x_{\mathrm{TB}}^2 + y_{\mathrm{TB}}^2}}\right), \tag{15}$$

and x_{TB}, y_{TB}, z_{TB} are the LoS vector components in $]^{\mathrm{L}}$, i.e., $[\bar{s}_{\mathrm{TB}}]^{\mathrm{L}} = [x_{\mathrm{TB}},\ y_{\mathrm{TB}},\ z_{\mathrm{TB}}]$. The guidance gains k_1 and k_2 aim at imposing the ballistic trajectory mimicking constraints.

Under the mild condition that the launch elevation angle $\theta(t_0) \in (0, \pi/2)$, the gain k_1 in (14) is determined by matching the initial heading error rate of the guided trajectory to that of the ballistic trajectory [10]. For the notation employed in this paper, k_1 takes the following form

$$k_1 = \frac{g(t_0)R_{\mathrm{go}}(t_0)}{V^2(t_0)\tan\gamma(t_0)}, \tag{16}$$

where the flight-path angle γ (cf. Fig. 3c) is given by

$$\gamma = \arctan\left(\frac{-w}{\sqrt{u^2 + v^2}}\right), \tag{17}$$

and the LoS separation R_{go}, henceforth referred to as range-to-go, is given by

$$R_{\text{go}} = \sqrt{x_{\text{TB}}^2 + y_{\text{TB}}^2 + z_{\text{TB}}^2}. \tag{18}$$

The gain k_2 is obtained by matching the final flight-path angle of the guided trajectory to that of the ballistic trajectory [10], i.e.,

$$k_2 = 2\frac{k_1\gamma(t_{\text{f}}) - \gamma(t_{\text{f}}) + \gamma(t_0)}{\gamma^2(t_{\text{f}})}. \tag{19}$$

Note that $\theta(t_0) = \gamma(t_0)$ holds for a perfectly aligned projectile inside the canon tube and, for stationary targets and perfect target hit, $\gamma(t_{\text{f}}) = \theta_{\text{O}}(t_{\text{f}})$.

In this paper, we suggest using (14) directly in the 3D PN structure of (9), while determining the guidance parameters k_1 and k_2 from a realistic 3D nonlinear simulation (cf. Section III.C.4). Compared to constant-gain PN, this strategy may help to better account for the curvature of the ballistic path. However, no expectations are made in terms of the ability to account for cross-range errors and deviations from the ideal ballistic path.

2. IBPN with Look-angle Constraints

For pursuers equipped with a strapdown seeker, Sharma and Ratnoo [11] proposed a modification to IBPN addressing the seeker's look-angle constraint. The resulting time-varying navigation gain can be expressed to have an identical structure as the one given in (14), but the two guidance gains, k_1 and k_2, take the following form

$$k_1 = 1 + \frac{\beta + \sqrt{\beta^2 + 4\beta\frac{\gamma(t_0)}{\gamma^*}}}{2}, \tag{20}$$

$$k_2 = \frac{\gamma^*\left(\beta - \sqrt{\beta^2 + 4\beta\frac{\gamma(t_0)}{\gamma^*}}\right) + 2\gamma(t_0)}{(\gamma^*)^2}, \tag{21}$$

where $\beta = 4\left(\sigma_{\max} - \gamma(t_0)\right)/\gamma^*$. The design objective of k_1 and k_2 is to generate acceleration commands which, at the final time t_{f}, lead to [11]

$$\lim_{t\to t_{\text{f}}} R_{\text{go}}(t) = \lim_{t\to t_{\text{f}}} \left(\gamma(t) - \gamma^*\right) = 0,$$

while satisfying

$$\sigma(t) \in [-\sigma_{\max},\, \sigma_{\max}], \qquad t \in [t_0, t_{\text{f}}).$$

Here, $\sigma = \gamma - \theta_{\text{O}}$ is the seeker's look-angle, $\sigma_{\max} > 0$ represents the maximum look-angle constraint, and $\gamma^* \in [-\pi, 0]$ denotes the desired impact angle. According to Sharma and Ratnoo [11], all impact angles $\gamma^* \in [-\pi, 0]$ can be achieved

with a bounded acceleration for any $\sigma_{\max}$ satisfying

$$\sigma_{\max} \geq \begin{cases} \gamma(t_0) & \text{if } \gamma^* \in [-2\gamma(t_0),\, 0], \\ -\frac{(\gamma^*)^2}{4(\gamma^*+\gamma(t_0))} & \text{if } \gamma^* \in [-\pi,\, -2\gamma(t_0)). \end{cases} \tag{22}$$

Similarly to the the IBPN case, the above guidance gains were derived for a planar engagement and under idealistic assumptions. We will use the resulting time-varying navigation gain $N(t)$ directly in the expression of the 3D PN guidance law of (9). As our goal is to mimic realistic ballistic trajectories, we will not impose any pre-defined impact angle constraint. Instead, we will set γ^* to be equal to $\gamma(t_\mathrm{f})$ obtained from a nonlinear simulation. Moreover, the value of $\sigma_{\max}$ has a direct influence on the resulting maneuverability requirements. Therefore, we will consider $\sigma_{\max}$ as a tuning parameter used to avoid actuator saturation and maximize projectile accuracy.

3. Realistic Ballistic Proportional Navigation

The proposed RBPN guidance law aims at addressing the shortcomings of PN, IBPN, and IBPN+C. Specifically, the aim is to mimic a realistic 3D ballistic trajectory by designing the time-varying navigation gain $N(t)$ such that the PN guidance law of (9) produces acceleration commands only when the actual projectile path deviates from the predicted nominal ballistic trajectory used for the computation of $N(t)$.

First, let us define $\boldsymbol{\omega}^{\mathrm{VE}}$ as the rotational velocity vector of the velocity vector $\boldsymbol{v}_{\mathrm{B}}^{\mathrm{E}}$ wrt Earth and $\boldsymbol{\omega}^{\mathrm{OE}}$ being the angular velocity vector of the LoS frame O wrt the inertial frame E. For an unguided projectile, the experienced acceleration normal to the projectile velocity can be expressed[‡] as a cross product of $\boldsymbol{\omega}^{\mathrm{VE}}$ and $\boldsymbol{v}_{\mathrm{B}}^{\mathrm{E}}$:

$$\tilde{\boldsymbol{a}}_{\mathrm{B}}^{\mathrm{E}} = \boldsymbol{\omega}^{\mathrm{VE}} \times \boldsymbol{v}_{\mathrm{B}}^{\mathrm{E}}. \tag{23}$$

Furthermore, the PN relation in 3D states that $\boldsymbol{\omega}^{\mathrm{VE}}$ must be made proportional to $\boldsymbol{\omega}^{\mathrm{OE}}$,

$$\boldsymbol{\omega}^{\mathrm{VE}} = N\boldsymbol{\omega}^{\mathrm{OE}}, \tag{24}$$

where N serves as the proportionality constant. Substituting (24) into (23) yields[§]

$$\tilde{\boldsymbol{a}}_{\mathrm{B}}^{\mathrm{E}} = N\boldsymbol{\omega}^{\mathrm{OE}} \times \boldsymbol{v}_{\mathrm{B}}^{\mathrm{E}}. \tag{25}$$

In order to mimic a realistic ballistic trajectory, we aim to find a proportionality constant $N(t)$ that attempts to make

[‡]We will skip the use of coordinate systems, unless necessary.

[§]Note that (25) resembles the PN equation of (9), but without the gravity bias term $\boldsymbol{g}$, which was added to the PN law in order to avoid the sagging tendency of the trajectory under seeker control [18].

the acceleration of the guided projectile (25) similar (in a L_2-norm sense) to the acceleration of the unguided projectile (23) for all time instances t during which the PN guidance law is actively engaged. This problem can be formulated as a minimization problem of the following cost function:

$$J = \frac{1}{2}\int_{t_s}^{t_f} \left\|\boldsymbol{\omega}^{\mathrm{VE}}(t) - N(t)\boldsymbol{\omega}^{\mathrm{OE}}(t)\right\|^2 \mathrm{d}t, \tag{26}$$

where $t_s \geq t_0$ denotes the start of the guidance law. It is obvious that in order to minimize J, it is sufficient to minimize the argument of the integral for all $t \in [t_s, t_f]$. Thus, for a fixed t, the first-order optimality condition can be expressed as

$$\frac{\partial \left\|\boldsymbol{\omega}^{\mathrm{VE}} - N\boldsymbol{\omega}^{\mathrm{OE}}\right\|^2}{\partial N} = -2\sum_{i=1}^{3}\left(\omega_i^{\mathrm{VE}} - N\omega_i^{\mathrm{OE}}\right)\omega_i^{\mathrm{OE}} = 0. \tag{27}$$

Solving the above equality wrt N yields the least squares solution, i.e., for $t \in [t_s, t_f]$ we have[¶]

$$N(t) = \underset{N(t)}{\arg\min}\, J = \frac{\sum_{i=1}^{3}\omega_i^{\mathrm{VE}}(t)\omega_i^{\mathrm{OE}}(t)}{\sum_{i=1}^{3}\left(\omega_i^{\mathrm{OE}}(t)\right)^2} = \frac{\boldsymbol{\omega}^{\mathrm{OE}}(t)\cdot\boldsymbol{\omega}^{\mathrm{VE}}(t)}{\|\boldsymbol{\omega}^{\mathrm{OE}}(t)\|^2}. \tag{28}$$

To compute (28), we need to obtain the off-line time-series for $\boldsymbol{\omega}^{\mathrm{OE}}$ and $\boldsymbol{\omega}^{\mathrm{VE}}$ in the same CS. To do this, we identify that the angular rate tensor $\boldsymbol{\omega}^{\mathrm{OE}}$ can be expressed in $]^{\mathrm{L}}$ as follows (cf. Fig. 3b)

$$\left[\boldsymbol{\omega}^{\mathrm{OE}}\right]^{\mathrm{L}} = \dot{\psi}_{\mathrm{O}}\left[\boldsymbol{e}_3\right]^{\mathrm{L}} + \dot{\theta}_{\mathrm{O}}\left[\bar{T}\right]^{\mathrm{X_O L}}\left[\boldsymbol{x}_{\mathrm{O2}}\right]^{\mathrm{X_O}} = \dot{\psi}_{\mathrm{O}}\begin{bmatrix}0\\0\\1\end{bmatrix} + \dot{\theta}_{\mathrm{O}}\begin{bmatrix}-\sin\psi_{\mathrm{O}}\\ \cos\psi_{\mathrm{O}}\\ 0\end{bmatrix} = \begin{bmatrix}-\dot{\theta}_{\mathrm{O}}\sin\psi_{\mathrm{O}}\\ \dot{\theta}_{\mathrm{O}}\cos\psi_{\mathrm{O}}\\ \dot{\psi}_{\mathrm{O}}\end{bmatrix}, \tag{29}$$

where the LoS elevation angle θ_{O} was defined in (15) and the LoS azimuth angle ψ_{O} is given by

$$\psi_{\mathrm{O}} = \arctan\left(\frac{y_{\mathrm{TB}}}{x_{\mathrm{TB}}}\right). \tag{30}$$

Alternatively, part of the formula (11) can be used to obtain $\boldsymbol{\omega}^{\mathrm{OE}}$ directly in $]^{\mathrm{L}}$. Similarly, $\boldsymbol{\omega}^{VE}$ in $]^{\mathrm{L}}$ can be expressed as (cf. Fig. 3c)

$$\left[\boldsymbol{\omega}^{VE}\right]^{\mathrm{L}} = \dot{\chi}\left[\boldsymbol{e}_3\right]^{\mathrm{L}} + \dot{\gamma}\left[T\right]^{\mathrm{LX_V}}\left[\boldsymbol{x}_{\mathrm{V2}}\right]^{\mathrm{X_V}} = \dot{\chi}\begin{bmatrix}0\\0\\1\end{bmatrix} + \dot{\gamma}\begin{bmatrix}-\sin\chi\\ \cos\chi\\ 0\end{bmatrix} = \begin{bmatrix}-\dot{\gamma}\sin\chi\\ \dot{\gamma}\cos\chi\\ \dot{\chi}\end{bmatrix}, \tag{31}$$

[¶]Here, "$\cdot$" signifies the dot product of two vectors.

where the flight-path angle γ was defined in (17) and the heading angle χ is given by

$$\chi = \arctan\left(\frac{v}{u}\right).$$

The time derivatives of the heading angle $\dot{\chi}$ and the flight-path angle $\dot{\gamma}$ can be either obtained by direct numerical differentiation of χ and γ, respectively, or alternatively by evaluating the following expressions:

$$\dot{\chi} = \frac{u\dot{v} - v\dot{u}}{u^2 + v^2}, \tag{32}$$

$$\dot{\gamma} = \frac{w(u\dot{u} + v\dot{v}) - \dot{w}(u^2 + v^2)}{V^2\sqrt{u^2 + v^2}}. \tag{33}$$

Here, the components $\dot{u}$, $\dot{v}$, and $\dot{w}$ are contained in $\left[\dot{\boldsymbol{v}}_{\mathrm{B}}^{\mathrm{E}}\right]^{\mathrm{B}'}$.

4. Implementation Details

The implementation of the IBPN or IBPN+C scheme is relatively straightforward. The two guidance gains k_1 and k_2 need to be computed off-line. Knowing the target's position, the projectile's initial conditions, such as $R_{\mathrm{go}}(t_0)$, $V(t_0)$, and $\gamma(t_0) = \theta(t_0)$, are easily obtained using ballistic tables. To obtain $\gamma(t_{\mathrm{f}})$, one could simply consider the fact that for an ideal ballistic trajectory, we have $\gamma(t_{\mathrm{f}}) = -\gamma(t_0)$. Alternatively, as suggested in Section III.C.1, consider a more realistic ballistic trajectory taking into account aerodynamic forces and moments and predict a more accurate estimate of the terminal impact angle $\gamma(t_{\mathrm{f}})$ using an off-line trajectory simulation of an un-guided projectile.

To implement the RBPN scheme, first we need to pre-calculate, parametrize, and store the navigation gain of (28) in a lookup table. Similarly as for IBPN(+C), the initial conditions for an unguided ballistic trajectory need to be found. Then, the 6-DoF nonlinear differential equations of (1)–(4) can be numerically integrated to obtain a nominal trajectory in terms of $\boldsymbol{\omega}^{\mathrm{OE}}$ and $\boldsymbol{\omega}^{\mathrm{VE}}$. Alternatively, a reduced-order 3-DoF (for fin-stabilized) or 4-DoF (for spin-stabilized) model can be considered. Once the trajectory estimate is obtained, the navigation gain can be parameterized using R_{go}, see (18), or by time-to-go t_{go} defined as $t_{\mathrm{go}} = t_{\mathrm{f}} - t$. Here, t is the integration time and t_{f} is the impact time obtained from the off-line simulation. Consequently, the discretized $R_{\mathrm{go}}(t_k)$-based or the $t_{\mathrm{go}}(t_k)$-based lookup table for $N(t_k)$ can be evaluated in-flight (e.g., by linear interpolation) using the estimates of R_{go} or t_{go} computed as:

$$\hat{R}_{\mathrm{go}} = \|\hat{\boldsymbol{s}}_{\mathrm{TE}} - \hat{\boldsymbol{s}}_{\mathrm{BE}}\|, \quad \text{or} \quad \hat{t}_{\mathrm{go}} = \frac{\hat{R}_{\mathrm{go}}}{\left|\hat{V}_{\mathrm{c}}\right|},$$

where the hat signifies in-flight estimates and V_{c} is the projectile-target closing speed defined as $V_{\mathrm{c}} = (\boldsymbol{s}_{\mathrm{TB}} \cdot \boldsymbol{v}_{\mathrm{TB}}^{\mathrm{E}})/\|\boldsymbol{s}_{\mathrm{TB}}\|$. Finally, Fig. 4 illustrates the integration of a R_{go}-based lookup table in the PN guidance law of (9).

Remark 1 *If the initial conditions used for the off-line trajectory simulation do not lead to a perfect target hit, the RBPN*

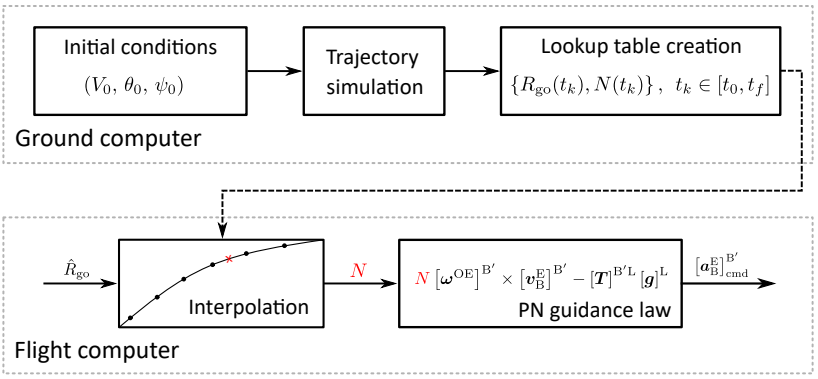

Fig. 4 Schematics of the RBPN guidance law with a $R_{\rm go}$ look-up table.

navigation gain $N(t)$ might have a spiky behavior as $t \to t_{\rm f}$. A remedy is to either bound the range of attainable values, i.e., $N_{\min} \le N(t) \le N_{\max}$, or to freeze the value of $N(t)$, $t \in [t_{\rm f} - \varepsilon, t_{\rm f}]$ to $N(t_{\rm f} - \varepsilon)$ for some small constant $\varepsilon > 0$.

IV. Results

A. Simulation Overview

In this section, we will compare the effectiveness of the three guidance schemes presented in Section III.C, when implemented for a spin-stabilized guided projectile equipped with a CCF [22]. For completeness, we also include the benchmark guidance law of PN and the current state-of-the-art guidance method for low-maneuverability guided projectiles, the ZEM guidance. The guidance laws are evaluated using a high-fidelity 7-DoF nonlinear simulator of a ballistic dual-spin guided projectile [23].

If an unguided projectile is launched with a given muzzle velocity $V_0 \triangleq V(t_0)$, initial spin rate $p_0 \triangleq p(t_0)$, elevation angle $\theta_0 \triangleq \theta(t_0)$, and azimuth angle $\psi_0 \triangleq \psi(t_0)$, it reaches a so-called ballistic impact point. However, due to uncertain launch/wind conditions and model parameters, a complete GNC loop is necessary to ensure a stationary target hit with a given CEP[‖] probability. In order to assess the guidance law performance solely, we assume that perfect navigation information is available to the guidance and autopilot modules.

The decoupled roll and pitch/yaw channel autopilots [22] were designed using $\mathcal{H}_\infty$ control techniques to achieve performance, robustness, and stability when the canard deflection angles $\delta_{\rm i}$ and their respective rates $\dot{\delta}_{\rm i}$ are within nominal operation ranges. Beyond these ranges, even though the validity/linearity of the aerodynamic model may not be guaranteed, anti-windup control laws were studied by the authors [24–26]. In this paper, the canard amplitude and rate saturation levels are set to $\delta^{\rm c}_{\rm sat} = \pm 30°$ and $\dot{\delta}^{\rm c}_{\rm sat} = \pm 100°/{\rm s}$.

For all guidance laws, a static flight envelop protection function (cf. Section III.A) is applied with the following values $\bar{n}_{\rm y} = \bar{n}_{\rm z} = 0.2$ g's. The value of the PN navigation gain was tuned via Monte Carlo (MC) simulations and was

[‖] The Circular Error Probable (CEP) is defined here as a circle, centered at the target's center T, whose radius includes 50% of the projectile's landing points. Analogously, $\text{CEP}_1\sigma$, $\text{CEP}_2\sigma$, and $\text{CEP}_3\sigma$ includes $1\sigma = 68.2\%$, $2\sigma = 95.4\%$, and $3\sigma = 99.7\%$ landing points, respectively.

set to $N = 2.23$. The value of $\sigma_{\max}$ for the IBPN+C guidance law was set to $\sigma_{\max} = \theta_0 (= \gamma_0) = 42°$. This value satisfies (22) and leads to smaller, slower-varying and more homogeneous amplitudes for the canard actuator control signals. Hence, the risk of actuator saturation is limited, while a good impact accuracy is maintained. In general, values $\sigma_{\max} > \theta_0$ result in higher amplitudes for the reference load factors and lead to more frequent canard saturations. For both, IBPN and IBPN+C, the value of $\gamma(t_f)$ was determined using the 6-DoF model presented in Section II.C. The same model has been used to construct the R_{go} based lookup table for the RBPN guidance law (cf. Section III.C.4). The implementation details and parameters of the ZEM guidance law can be found in [14].

B. Nominal Ballistic Trajectory

Before evaluating the guidance laws in a MC setting, we first simulate a nominal ballistic trajectory. A nominal trajectory can be defined as an unguided ballistic flight without any uncertainties.

For the initial conditions presented in Table 1 and for a target located at 24km downrange from the projectile launch point, the resulting ballistic trajectory shown in Fig. 5a represents a perfect target hit. To better appreciate the drift in the crossrange direction due to the yaw of repose effect, the resulting trajectory was coordinated to the Canon's $]^C$ CS. Here, the x-axis is referred to as downrange, the y-axis as crossrange, and the z-axis represents the altitude. The associated coordinate transformation matrix from $]^L$ to $]^C$ is given by

$$[\boldsymbol{T}]^{CL} = \begin{bmatrix} \cos\psi_0 & \sin\psi_0 & 0 \\ -\sin\psi_0 & \cos\psi_0 & 0 \\ 0 & 0 & 1 \end{bmatrix} \tag{34}$$

Figure 5b illustrates the various navigation gain variations as a function of range-to-go. These gains were computed in an open-loop fashion from the available kinematic variables corresponding to the nominal ballistic trajectory and the initial conditions presented in Table 1.

Table 1 Initial conditions of the nominal trajectory.

State	Value	Unit
Initial velocity (V_0)	940	m/s
Initial spin rate (p_0)	305	Hz
Launch elevation angle (θ_0)	42	°
Launch azimuth angle (ψ_0)	1.69	°

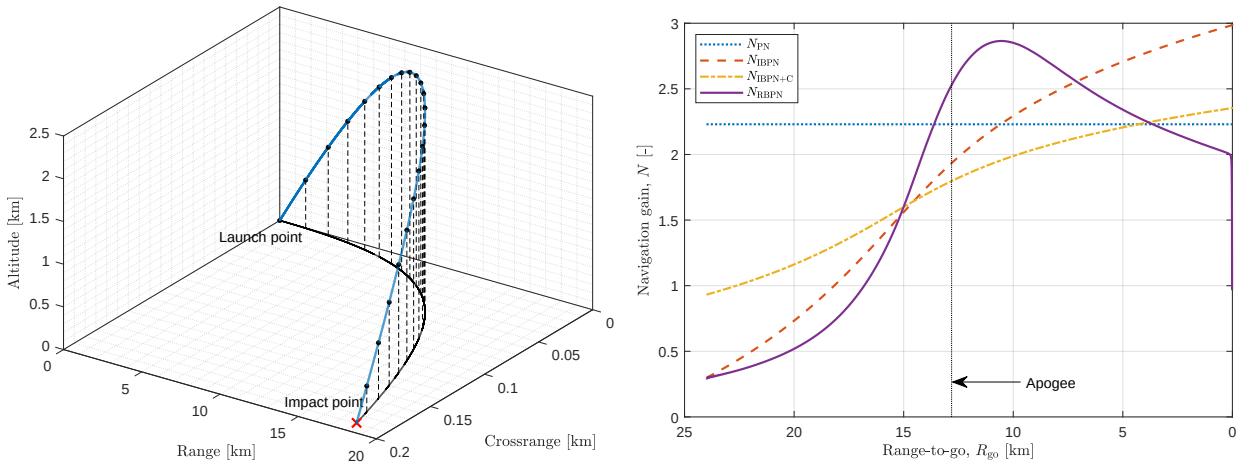

(a) Nominal ballistic trajectory and impact point.

(b) Navigation gain variation for a perfect hit.

Fig. 5 Nominal ballistic trajectory simulation results.

C. Monte Carlo Results

To demonstrate the effectiveness of the proposed methods, we perform 2000 MC simulations for each guided case as well as for the pure ballistic case. The initial conditions presented in Table 1, as well as some aerodynamic coefficients (longitudinal force C_{X}, normal force slope $C_{\mathrm{N}\alpha}$) and environmental parameters (pressure P, temperature T, longitudinal wind u_{w}, lateral wind v_{w}) are altered according to a normally distributed random uncertainties summarized in Table 2.

Table 2 Parameter uncertainties.

Parameter	1σ value	Unit
V_0	5	m/s
θ_0	1.5	mils (NATO)
ψ_0	2.5	mils (NATO)
C_{X}	1	%
$C_{\mathrm{N}\alpha}$	3	%
P, T	0.4	%
$u_{\mathrm{w}}, v_{\mathrm{w}}$	3.5	m/s

For the guided cases, the entire flight is decomposed into two flight phases: a) ballistic open-loop phase and b) closed-loop guided phase. At the start of the closed-loop phase at time t_{s}, the pitch-yaw guidance and control are initiated. We will investigate two start times, namely $t_{\mathrm{s}} = 23$ s and $t_{\mathrm{s}} = 60$ s. The latter start time results in approximately less than 21 s of guided phase. From this flight point onwards, the resulting trajectory resembles a quasi-straight line. Even though the determination of an optimal starting time for the guided phase is an important topic per se, the authors tend to believe that due to the particularity of the considered system (i.e. spin-stabilized projectile with very limited control authority and hence maneuverability), this ought to start at the earliest time possible, for example immediately after the GPS signal is available and any initial cannon-induced trajectory oscillations and transients have died out.

The simulation results in Fig. 6 and Fig. 7 represent the relative impact distributions for $t_s = 60$ s and $t_s = 23$ s, respectively. These results are also summarized in Table 3. Fig. 8 shows the Cumulative Distribution Function (CDF) of the maximal necessary canard deflection angle during the guided phase. As can be seen from Fig. 6a, the total ballistic dispersion that needs to be corrected by the guidance is more than ±1000 m in downrange and ±500 m in crossrange.

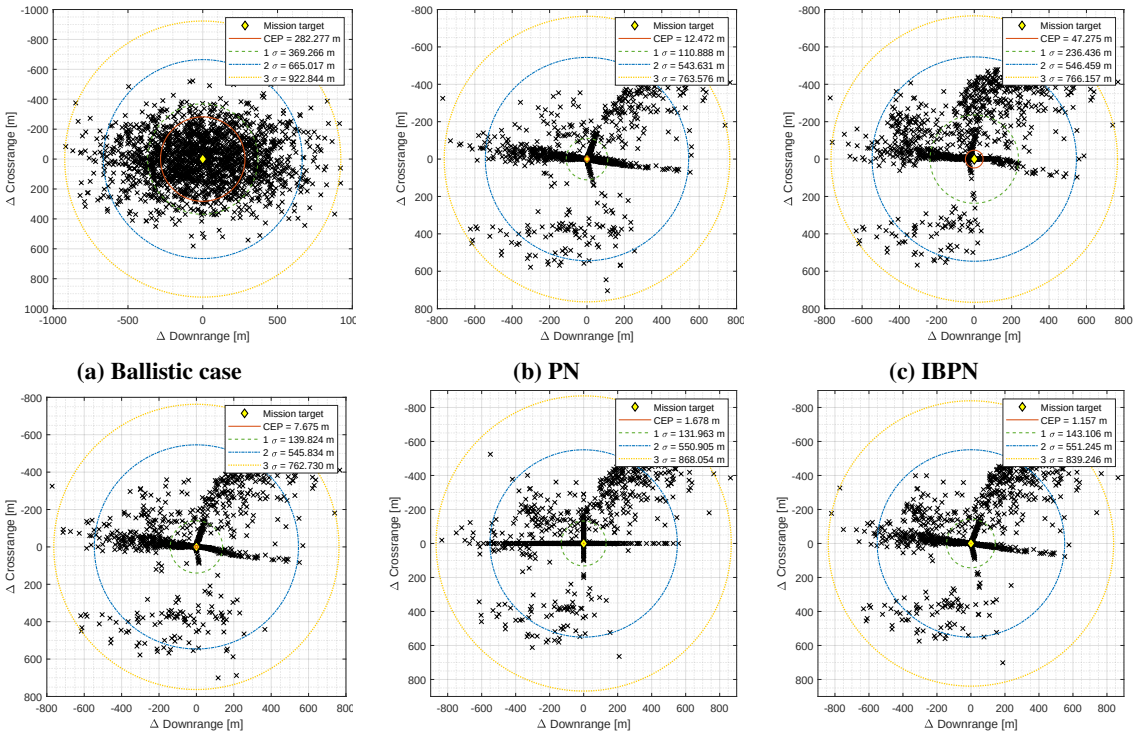

(a) Ballistic case **(b) PN** **(c) IBPN**

(d) IBPN+C **(e) ZEM** **(f) RBPN**

Fig. 6 Relative impact distributions for guidance starting at $t_s = 60$ s.

Table 3 Summary of the Monte Carlo run results in [m].

Evaluation metric	CEP		$CEP_{1\sigma}$		$CEP_{2\sigma}$		$CEP_{3\sigma}$	
Guidance starts	$t_s = 60$ s	$t_s = 23$ s	$t_s = 60$ s	$t_s = 23$ s	$t_s = 60$ s	$t_s = 23$ s	$t_s = 60$ s	$t_s = 23$ s
Ballistic case	282.277		369.266		665.017		922.844	
PN [18]	12.472	1848.352	110.888	2011.929	543.631	2408.394	763.576	2718.922
IBPN [10]	47.275	400.581	236.436	504.082	546.459	880.248	766.157	1217.010
IBPN+C [11]	7.675	401.183	139.824	496.888	545.834	805.346	762.730	1257.186
ZEM [14]	1.678	0.008	131.963	0.013	550.905	0.028	868.054	0.109
RBPN	1.157	0.002	143.106	0.002	551.245	0.004	839.246	0.006

As it can be inferred from Table 3, all evaluated guidance laws are able to reduce the dispersion below 50 m of CEP when engaging the guidance at $t_s = 60$ s. However, only RBPN and ZEM permit an earlier start of the guidance, yielding to a significant performance gain, especially for the $CEP_{3\sigma}$ metric. This behavior is likely to be attributed to the ability of these guidance laws to fully exploit the built-in (i.e., by design) information about the nominal ballistic

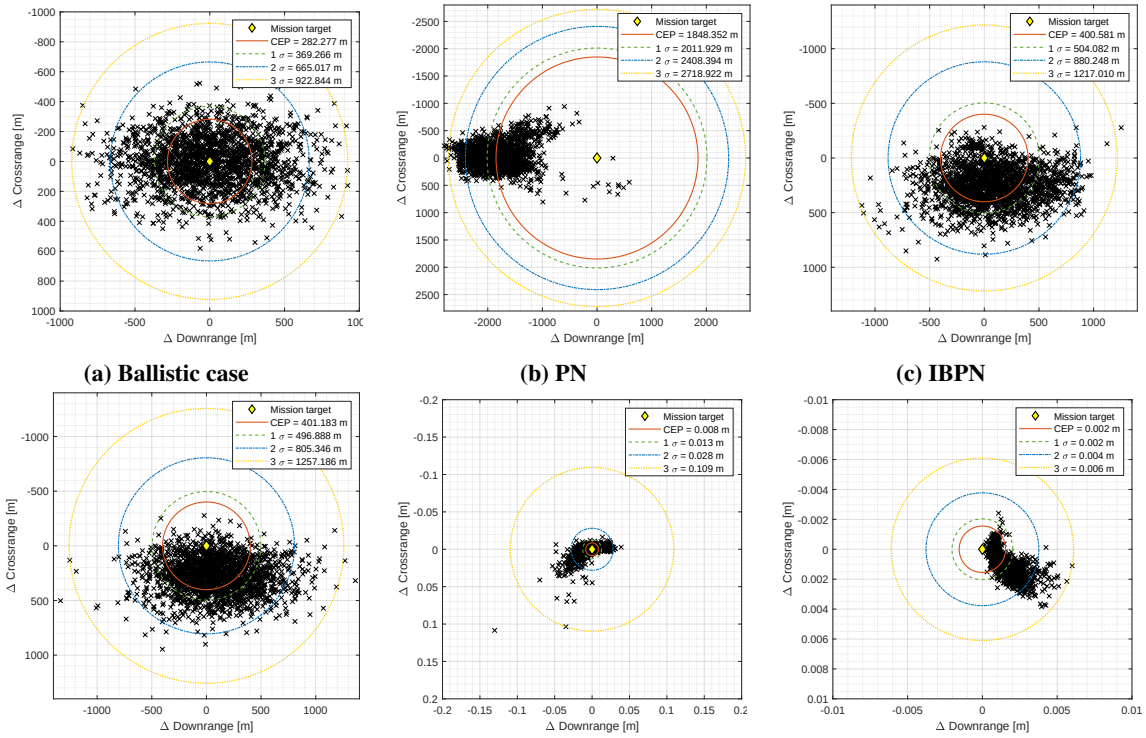

(a) Ballistic case **(b) PN** **(c) IBPN**

(d) IBPN+C **(e) ZEM** **(f) RBPN**

Fig. 7 Relative impact distributions for guidance starting at $t_s = 23$ s.

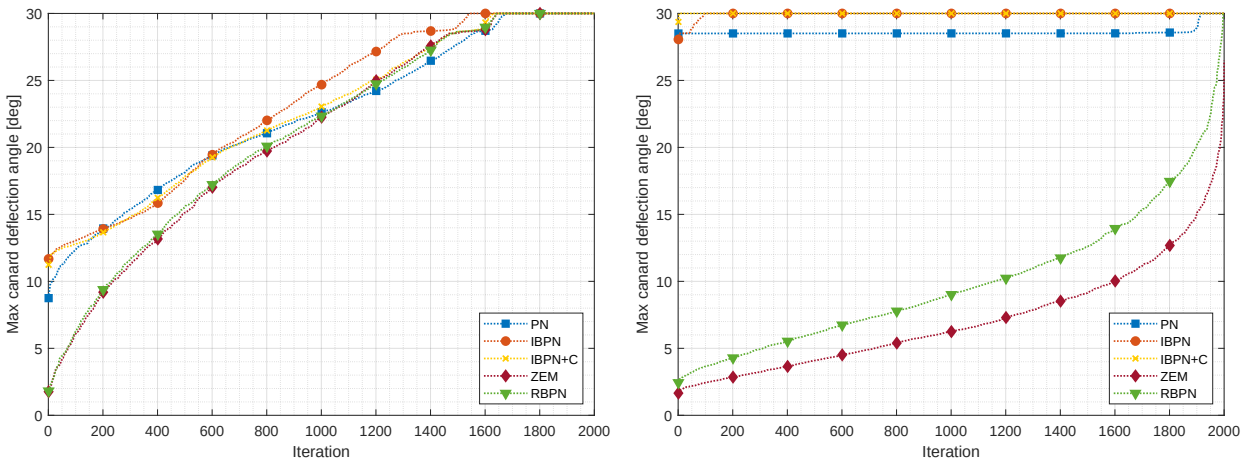

(a) Guidance starts at $t_s = 60$ s. **(b) Guidance starts at $t_s = 23$ s.**

Fig. 8 CDF of the maximal canard deflection angle.

trajectory and make the necessary trajectory corrections earlier in the guidance phase. Consequently, as can be observed in Fig. 8b, earlier trajectory corrections help to avoid actuator saturations. Surprisingly, the same observation cannot be made for IBPN and IBPN+C. Despite the fact that both of these schemes aim at taking into account the (ideal) ballistic trajectory of the projectile, the performance significantly drops when compared to the deferred start of $t_s = 60$ s. On the other hand, the earlier start of PN, IBPN, and IBPN+C considerably deteriorate the performance, even when compared

to the unguided ballistic case.

Figure 8a suggests that a deferred start of the guidance can lead to actuator saturations for all guidance strategies. This is likely a consequence of not having enough time to make the necessary trajectory corrections. Nevertheless, the guidance laws of PN, IBPN, and IBPN+C achieve a similar level of performance as RBPN and ZEM. This is likely to be attributed to the fact that as the projectile approaches the target, the remaining trajectory is closer to the straight line, hence the underlying design assumptions of these guidance laws become more and more valid.

V. Conclusions

The simulation results of a dual-spin projectile suggest that, when compared to the legacy PN guidance law, the heuristic adaptations of IBPN and IBPN+C to the three-dimensional guidance case can provide an extra performance boost at the expense of added complexity of having to measure the LoS elevation angle during the flight. On the other hand, the newly proposed RBPN guidance law demonstrates, in general, better performance than the state-of-the-art ZEM guidance law. Moreover, the on-board computational complexity of RBPN is considerably lower than the ZEM which, at each discrete time step, performs an online trajectory simulation on-board. In contrast to this, the RBPN scheme only consists of a simple PN structure augmented with a two-dimensional lookup table to select the appropriate value of the PN navigation gain. The navigation gain is computed off-line and allows to fully take into account the true curvature of the nominal ballistic trajectory. All these aspects additionally allow the RBPN to be engaged early enough in the ballistic phase to command necessary trajectory corrections and avoid potential actuator limits violations.

References

[1] Fresconi, F., "Guidance and Control of a Projectile with Reduced Sensor and Actuator Requirements," *Journal of Guidance, Control, and Dynamics*, Vol. 34, No. 6, 2011, pp. 1757–1766. https://doi.org/10.2514/1.53584.

[2] Theodoulis, S., Gassmann, V., Wernert, P., Dritsas, L., Kitsios, I., and Tzes, A., "Guidance and Control Design for a Class of Spin-Stabilized Fin-Controlled Projectiles," *Journal of Guidance, Control, and Dynamics*, Vol. 36, No. 2, 2013, pp. 517–531. https://doi.org/10.2514/1.56520.

[3] Gagnon, E., and Lauzon, M., "Course Correction Fuze Concept Analysis for In-Service 155 mm Spin-Stabilized Gunnery Projectiles," *AIAA Guidance, Navigation and Control Conference and Exhibit*, 2008. https://doi.org/10.2514/6.2008-6997.

[4] Jitpraphai, T., and Costello, M., "Dispersion Reduction of a Direct Fire Rocket Using Lateral Pulse Jets," *Journal of Spacecraft and Rockets*, Vol. 38, No. 6, 2001, pp. 929–936. https://doi.org/10.2514/2.3765.

[5] Rogers, J., and Costello, M., "Design of a Roll-Stabilized Mortar Projectile with Reciprocating Canards," *Journal of Guidance, Control, and Dynamics*, Vol. 33, No. 4, 2010, pp. 1026–1034. https://doi.org/10.2514/1.47820.

[6] Gagnon, E., and Vachon, A., "Efficiency Analysis of Canards-Based Course Correction Fuze for a 155-mm Spin-Stabilized Projectile," *Journal of Aerospace Engineering*, 2016, pp. 1–10. https://doi.org/10.1061/(ASCE)AS.1943-5525.0000634.

[7] Yuan, L. C., "Homing and Navigational Courses of Automatic Target Seeking Devices," *Journal of Applied Physics*, Vol. 19, No. 12, 1948, pp. 1122–1128. https://doi.org/10.1063/1.1715028.

[8] Guo, Q., Song, W., Wang, Y., and Lu, Z., "Guidance Law Design for a Class of Dual-Spin Mortars," *International Journal of Aerospace Engineering*, 2015. https://doi.org/10.1155/2015/952076.

[9] Zhang, Y., Gao, M., Yang, S., and Fang, D., "An adaptive proportional navigation guidance law for guided mortar projectiles," *The Journal of Defense Modeling and Simulation*, Vol. 13, No. 4, 2016, pp. 467–475. https://doi.org/10.1177/1548512916647810.

[10] Sharma, Y. R., and Ratnoo, A., "Guidance law for mimicking short-range ballistic trajectories," *Proceedings of the Institution of Mechanical Engineers, Part G: Journal of Aerospace Engineering*, Vol. 233, No. 11, 2019, pp. 4176–4190. https://doi.org/10.1177/0954410018817424.

[11] Sharma, Y. R., and Ratnoo, A., "A Bearings-Only Trajectory Shaping Guidance Law with Look-Angle Constraint," *IEEE Transactions on Aerospace and Electronic Systems*, Vol. 55, No. 6, 2019, pp. 3303–3315. https://doi.org/10.1109/TAES.2019.2906090.

[12] Yang, S., "Impact-Point-Based Guidance of a Spinning Artillery Rocket Using Canard Cyclic Control," *Journal of Guidance, Control, and Dynamics*, Vol. 43, No. 10, 2020, pp. 1975–1982. https://doi.org/10.2514/1.G004956.

[13] Wang, Y., Song, W., Fang, D., and Guo, Q., "Guidance and Control Design for a Class of Spin-Stabilized Projectiles with a Two-Dimensional Trajectory Correction Fuze," *International Journal of Aerospace Engineering*, 2015. https://doi.org/10.1155/2015/908304.

[14] Proff, M., and Theodoulis, S., "Study of Impact Point Prediction Methods for Zero-Effort-Miss Guidance: Application to a 155 mm Spin-Stabilized Guided Projectile," *5th CEAS Conference on Guidance, Navigation and Control*, 2019.

[15] Lieske, R. F., and Reiter, M. L., "Equations of Motion for a Modified Point Mass Trajectory," Tech. rep., U.S. Army Ballistic Research Laboratory, Aberdeen Proving Ground, MD, March 1966. BRL Rept. No. 1314, AD 485869.

[16] Tipàn, S., Theodoulis, S., Thai, S., and Proff, M., "Nonlinear Dynamic Inversion Flight Control Design for Guided Projectiles," *Journal of Guidance, Control, and Dynamics*, Vol. 43, No. 5, 2020, pp. 975–980. https://doi.org/10.2514/1.G004976.

[17] Wernert, P., Theodoulis, S., and Morel, Y., "Flight Dynamics Properties of 155mm Spin-Stabilized Projectiles Analyzed in Different Body Frames," *AIAA Atmospheric Flight Mechanics Conference*, Portland, USA, 2010. https://doi.org/10.2514/6.2010-7640, AIAA 2010-7640.

[18] Zipfel, P. H., *Modeling and Simulation of Aerospace Vehicle Dynamics*, 2nd ed., AIAA Education Series, AIAA, Reston, VA, 2007. https://doi.org/10.2514/4.862182, chapter 2 and 9.

[19] Sève, F., and Theodoulis, S., "Design of an H_∞ Gain-Scheduled Guidance Scheme for a Guided Projectile," *Journal of Guidance, Control, and Dynamics*, Vol. 42, No. 11, 2019, pp. 2399–2417. https://doi.org/10.2514/1.G004317.

[20] Zarchan, P., *Tactical and Strategic Missile Guidance*, 6^{th} ed., Progress in Astronautics and Aeronautics, Vol. 239, AIAA, Reston, VA, 2012. https://doi.org/10.2514/4.868948, chapter 2.

[21] Shneydor, N., *Missile Guidance and Pursuit: Kinematics, Dynamics and Control*, Horwood Publishing, Chichester, England, 1998. Chapter 5.

[22] Theodoulis, S., Sève, F., and Wernert, P., "Robust Gain-Scheduled Autopilot Design for Spin-Stabilized Projectiles with a Course-Correction Fuze," *Aerospace Science and Technology*, Vol. 42, 2015, pp. 477–489. https://doi.org/10.1016/j.ast.2014.12.027.

[23] Sève, F., Theodoulis, S., Zasadzinski, M., Boutayeb, M., and Wernert, P., "Nonlinear Flight Simulator of a Canard-Guided Spin-Stabilized Projectile," *3rd CEAS EuroGNC Conference*, Warsaw, Poland, 2015, pp. 1–20.

[24] Thai, S., Theodoulis, S., Roos, C., Biannic, J.-M., and Proff, M., "Gain-Scheduled Autopilot Design with Anti-Windup Compensator for a Dual-Spin Canard-Guided Projectile," *IEEE Conference on Control Technology and Applications*, Montreal, Canada, 2020. https://doi.org/10.1109/CCTA41146.2020.9206311.

[25] Thai, S., Roos, C., Biannic, J.-M., and Theodoulis, S., "An Interpolated Model Recovery Anti-Windup for a Canard-Guided Projectile Subject to Uncertainties," *2021 European Control Conference (ECC)*, 2021, pp. 1693–1698. https://doi.org/10.23919/ECC54610.2021.9655059.

[26] Thai, S., "Advanced Anti-Windup Flight Control Algorithms for Fast Time-Varying Aerospace Systems," Ph.D. thesis, 2021. URL http://www.theses.fr/2021ESAE0040.